Article

Selective Turn-On Fluorescence Sensing of Cyanide Using the Pyridoxal Platform of a Ni(II) Complex

Antu Mondal and Shyamal Kumar Chattopadhyay*

Cite This: *ACS Omega* 2022, 7, 40941−40949

Read Online

ACCESS | Metrics & More | Article Recommendations | SI Supporting Information

ABSTRACT: Cyanide is a very toxic pollutant to aquatic life and the environment. Analytical methods for the quantitative assay of cyanide, which are rapid, sensitive (low limit of detection), and cost-effective, are in great demand. Colorimetric and fluorometric methods are ideally suited for this purpose. In this report, we describe a Ni(II) complex containing a pyridoxal platform for the rapid and sensitive fluorometric estimation of cyanide. The square-planar Ni(II) complex, $[Ni(L)(N_3)] \cdot 3H_2O$, where the ligand LH = 4-[(2-dimethylamino-ethylimino)-methyl]-5-hydroxymtheyl-2-methyl-pyridin-3-ol, a Schiff base formed between pyridoxal and (2-dimethylamino)ethyl amine, was synthesized and characterized by various spectroscopic techniques as well as by single-crystal X-ray structure determination. The complex was found to selectively bind CN^- in the presence of other biologically important anions such as F^-, Cl^-, Br^-, I^-, OAc^-, S^{2-}, NO_3^-, PO_4^{3-}, SO_4^{2-}, and $H_2PO_4^-$ in tris-HCl/NaCl buffer [pH = 7.4], and it can be monitored by fluorescence turn-on or by UV−visible spectroscopy. The binding constant of the complex with CN^- was estimated to be 2.046×10^{14} M^{-2} and the limit of detection (LOD) was 9 nM, the LOD being considerably lower than the maximum permissible level of cyanide ions (1.9 μM) in drinking water, as recognized by the World Health Organization (WHO). The effects of pH and temperature on the sensing are also investigated. The Ni(II) complex is also found to bind to calf-thymus DNA very strongly, and the apparent binding constant (K_{app}) was determined to be 1.33×10^7 M^{-1} by the fluorescence quenching of the ethidium bromide−DNA adduct by the complex.
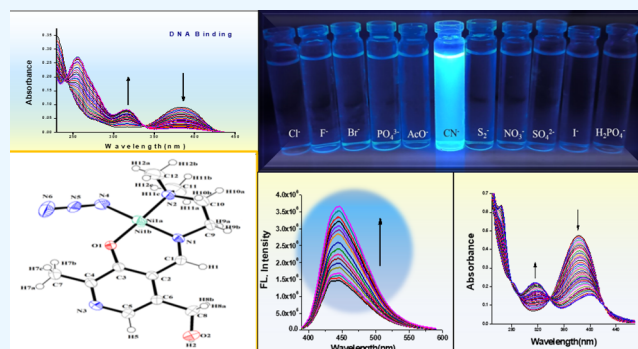
1. INTRODUCTION

Nickel is one of the metal ions that play a significant role in the biology of microbes and plants, where it is used in certain cellular processes, especially nitrogen metabolism.[1,2] Both prokaryotic and eukaryotic creatures are affected by the loss of nickel homeostasis.[3] An adult human consumes 300−600 μg of nickel per day on average.[4,5] Excessive nickel intake may cause nickel toxicity, which may result in serious health effects ranging from asthma and allergic dermatitis to lung cancer and even nasal sinus cancer.[6,7] Again, the use of nickel compounds for industrial and commercial purposes is quite extensive, viz., in Ni−Cd batteries, in the preparation of pigments for painting, in electroplating, as a welding material, and as a catalyst in many chemical reactions. There are several chemical reactions in which multiple nickel complexes act as catalysts, e.g., the epoxidation reaction of terminal, aliphatic, and aromatic olefins,[8,9] ester hydrolysis at ambient temperatures,[10] ethylene oligomerization,[11,12] and olefin polymerization.[13] There is, however, little information available about the use of nickel complexes to detect typical toxic ions such as cyanide ions.

Among all pollutants in the environment, cyanide is extremely harmful and immensely toxic to living creatures. Inorganic cyanides, mainly of potassium and sodium, are highly water soluble. Thus, when consumed, they quickly form solutions in the stomach, which swiftly enter the bloodstream and circulate throughout the entire body within a very short time. Cyanides and hydrocyanic acid (HCN) are toxic to living animals, in particular mammals, which is ascribed to their irreversible reaction and binding to the $cyta_3$ of cytochrome oxidase, thereby hindering the respiratory cycle and preventing the assimilation of oxygen. At higher doses, it can also attack other heme-proteins such as hemoglobin and myoglobin. As oxygen is essential for the proper functioning of the brain and muscles, cyanide poisoning can lead to death within a short span of time. Furthermore, it can disrupt many functions of the body, such as those of the central nervous system as well as the visual, cardiovascular, endocrine, and metabolic systems. The harmful consequence of cyanide also affects various industries such as metal trade, X-ray film recovery, electroplating, mining, and

Scheme 1. Schematic Illustration of the Synthesis of the Ni(II) Complex
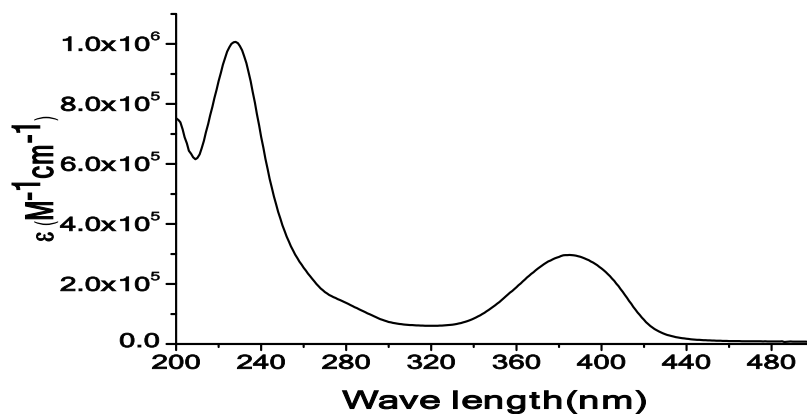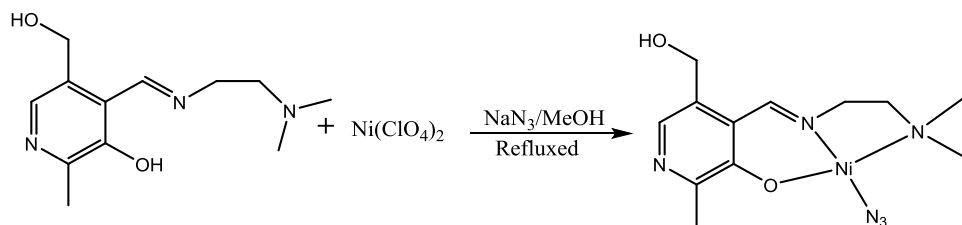
Figure 1. UV−vis spectrum of the complex ([Ni^{II}(L)(N$_3$)]·3H$_2$O) (Tris buffer).

jewelry manufacturing. These make cyanide the deadliest toxic pollutant in the environment.[14−23]

Several analytical methods such as spectroscopies (emission spectroscopy/atomic absorption), electrochemical methods (anodic stripping voltammetry), mass spectrometry, inductively coupled plasma spectrometry, and flame photometry have been reported[24−32] for cyanide assay. Generally, these processes involve multistep procedures with hazardous sample pretreatments or the use of a high proportion of organic solvents or sophisticated instrumentation. Anions can be measured qualitatively and quantitatively using chemosensors developed for the recognition of anions.[33−36] Specifically, the development of chromogenic compounds that yield a very fast response to the presence of analytes with visible color changes would provide an opportunity in the field of rapid detection of this lethal ion in aqueous solvents.

Although there have been numerous reports on cyanide sensors so far, many of them suffer from some serious problems, e.g., not operating fully in aqueous solutions, requiring exhaustive synthetic protocols, lack of selectivity toward cyanide, and, in some cases, a very high limit of detection in the case of some sensors. Thus, it is imperative to prepare a reliable sensor material that can selectively detect cyanide anions in aqueous solutions by both chromogenic and fluorogenic pathways, has a low detection limit, and can yield semiquantitative information for naked eye detection. Copper complexes of a variety of ligands have been extensively used for this purpose because of the high affinity of copper ions toward cyanide.[37−40] Attempts have also been made in some cases to understand the interaction of cyanide with copper ions by density functional theory (DFT) calculations.[39,40] However, the use of metal complexes of other first transition series metal ions such as iron and nickel are relatively scarce.[41]

Herein, we report a Ni(II) metal complex of a Schiff base ligand of pyridoxal, which is able to selectively detect cyanide ion in an aqueous medium.

2. EXPERIMENTAL SECTION

2.1. Synthesis of the Complex [Ni(L)(N$_3$)]·3H$_2$O. The *in situ* preparation of the ligand (LH) was performed by following a procedure described in an earlier study.[42] To a solution of Ni(ClO$_4$)$_2$·6H$_2$O (0.365 g, 1 mmol) in methanol, the *in situ*-prepared ligand (1 mmol) solution was added dropwise. The reaction mixture was then refluxed for 1 h with the subsequent addition of NaN$_3$ (0.130 g, 2 mmol), and then the reflux was continued for another 3 h. After filtering the brown solution, the filtrate was placed in a beaker at room temperature for slow evaporation. A few days later, brown crystals of [Ni^{II}(L)(N$_3$)]· 3H$_2$O appropriate for X-ray structure determination were collected.

Yield: 316 mg (81%). Anal calcd for C$_{12}$H$_{24}$N$_6$O$_5$Ni (M.W. 391): H, 6.19; C, 36.86; N, 21.49. Found: H, 6.18; C, 36.84; N, 21.50. Mass: ESI-positive ion mode-*m/z*: 394 [Ni^{II}(L)(N$_3$) + K + H$_3$O$^+$] (Figure S1). ^{1}H NMR (DMSO, 400 MHz): δH 7.86 (1H, s), 7.91 (1H, s), 3.31−3.24 (2H, m), 3.08 (2H, s), 2.63− 2.56 (2H, m), 2.28 (3H, s), 2.18 (6H, s) (Figure S2). Electronic spectrum was recorded in tris-HCl buffer having pH 7.4: λ_{max}/ nm (ε_{max}/M^{-1}cm^{-1}): 228(10070), 384(2959); selected IR bands (cm^{-1}): 2140 (ν_{N_3}), 1558($\nu_{C=N}$), 3286(ν_{O-H}), 3652- (ν_{H_2O}).

2.2. X-ray Crystallography. The diffractometer used here to collect single-crystal X-ray data of the Ni(II) complex at 295(2) K was a Bruker D8-Venture (microfocus source of Mo Kα radiation (0.71073 Å)). Direct methods were used to correct and interpret the data. Using SHELXL-2018/3, refinement was performed on F^2 using full-matrix least squares.[43,44] To refine hydrogen atoms, isotropic displacement parameters were used. To refine the non-hydrogen atoms, anisotropic displacement parameters were used. There was some disorder in the Ni atom. After refinement, the occupancies of Ni1A and Ni1B were 0.6 and 0.4, respectively (the split option was used). The methyl groups as well as one of the water molecules (O5(H5A, H5B))

were refined as rotating groups. Important crystallographic data are summarized in Table S1. Selected bond angles and distances are presented in Table S2. We submitted the crystal data to the CCDC with submission number 2 166 698.

2.3. DNA-Binding Experiment. The DNA binding study of the complex was carried out both by absorption spectroscopy and fluorescence spectroscopy. The details of the experiment are provided in the Supporting Information.

3. RESULTS AND DISCUSSION

3.1. Synthesis of the Complex. The Schiff base ligand was synthesized by the reaction of the neutral pyridoxal (obtained by
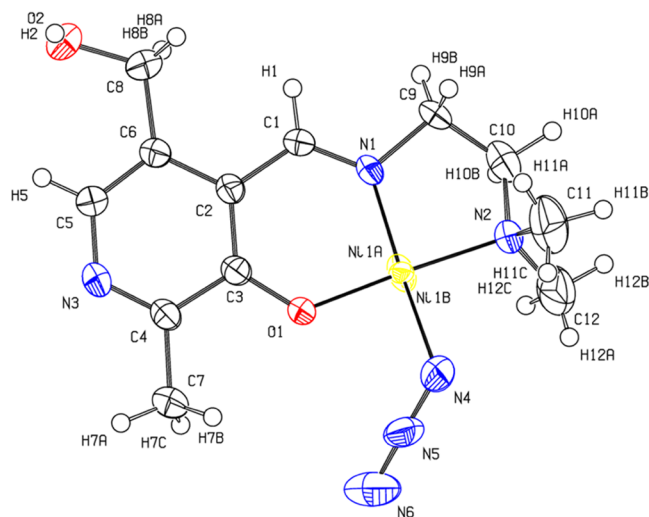

Figure 2. ORTEP diagram (ellipsoids are drawn with 50% probability) of the complex molecule of $[Ni^{II}(L)(N_3)] \cdot 3H_2O$.

in situ neutralization of a methanolic solution of pyridoxal hydrochloride with aqueous KOH) and (2-dimethylamino)-ethyl amine in methanol. The reaction of the *in situ*-generated ligand with nickel(II) perchlorate in methanol (1:1 molar ratio) followed by the addition of an aqueous solution of NaN_3 in 1:2 molar ratio and refluxing of the mixture for 3 h afforded a brown-colored complex (Scheme 1).

3.2. IR Study. A sharp peak at 2140 cm^{-1} in the IR spectra of the complex indicates the presence of azide (N_3) in the complex.

The $v_{(C=N)}$ band was observed at 1558 cm^{-1} in the complex compared with 1628 cm^{-1} observed in the free ligand. A sharp peak at 3286 cm^{-1} is probably due to $v_{(O-H)}$. A very broad band around 3652 cm^{-1} indicated the presence of lattice water (Figure S3).

3.3. Electronic Spectra. In the Ni(II) complex, a band at 228 nm was assigned to the $\pi \to \pi^*$ transition of the ligand, and an intense band at around 384 nm was assigned to an LMCT transition from the phenolate oxygen of pyridoxal to Ni(II) (Figure 1).

3.4. Description of the X-ray Crystal Structure. An ORTEP diagram of the complex along with the atom-numbering scheme is given in Figure 2. It shows that the Ni(II) complex has a square-planar geometry. A detailed description of the X-ray crystal structure is provided in the Supporting Information.

3.5. DNA-Binding Study. *3.5.1. UV–vis Spectral Study.* UV–vis spectrophotometry was performed to determine the binding capacity of the complex toward calf thymus DNA (Figure 3a). Both the nickel(II) complex (5×10^{-6} M) and the calf thymus DNA (5×10^{-5} M) solutions were prepared using aqueous Tris buffer (pH = 7.4). The change in the absorption spectra was recorded after the successive addition of calf thymus DNA (5×10^{-5} M) into the solution of the complex (5×10^{-6} M). After the addition, we found a hypochromic change of the absorption band of the complex at 384 nm; on the other hand, we also found a new band developing at 316 nm, which shows hyperchromism. The intrinsic binding constant K_b for DNA binding by the complex was calculated from the ratio of the slope to the intercept in the plot of $[DNA]/(\varepsilon_a - \varepsilon_f)$ versus $[DNA]$ to be 7.54×10^6 M^{-1} using the hypochromism of the 384 nm band (Figure 3b).

3.5.2. Fluorescence Binding Analysis. Normally, DNA has a very weak intensity of fluorescence, but the intensity could be greatly increased by the specific intercalation of EB into DNA base pairs.[45,46] The addition of a strong intercalating complex into the EB−DNA adduct causes quenching of the fluorescence, as they tenaciously bind with DNA and displace EB from DNA.[47] The fluorescence intensity of the DNA−EB mixture started to decrease significantly with the addition of our Ni(II) complex (Figure 4), indicating that the complex displaced EB from the DNA−EB system and itself bound to DNA.[48] The Stern−Volmer equation can be used to fit the fluorescence quenching data: $I^0/I = 1 + K_{sv}[Q]$, where K_{sv}, $[Q]$, I, and I^0 are the quenching constant, the quencher (complex) concentration,
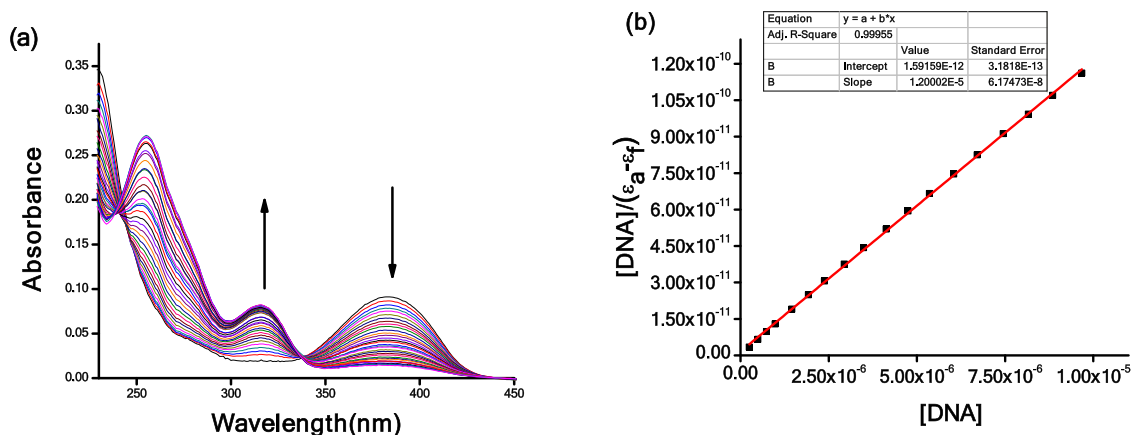

Figure 3. (a) Changes in the absorption spectra of the complex (5×10^{-6} M) on the incremental addition of ct-DNA (5×10^{-5} M) in tris buffer at room temperature. (b) Plot of $[DNA]/(\varepsilon_a - \varepsilon_f)$ versus $[DNA]$ representing the titration of DNA and the Ni(II) complex.
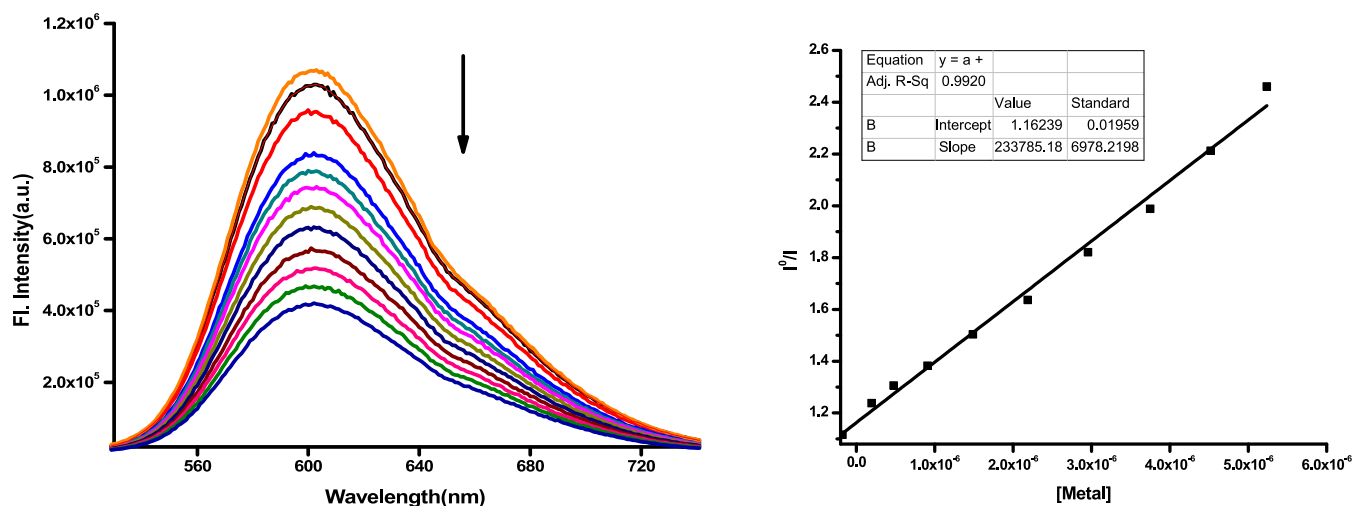
Figure 4. Plot of the fluorescence titration data of the complex with ethidium bromide−DNA in 0.01 M Tris buffer (λ_{ex} = 520 nm) and the corresponding Stern−Volmer plot.
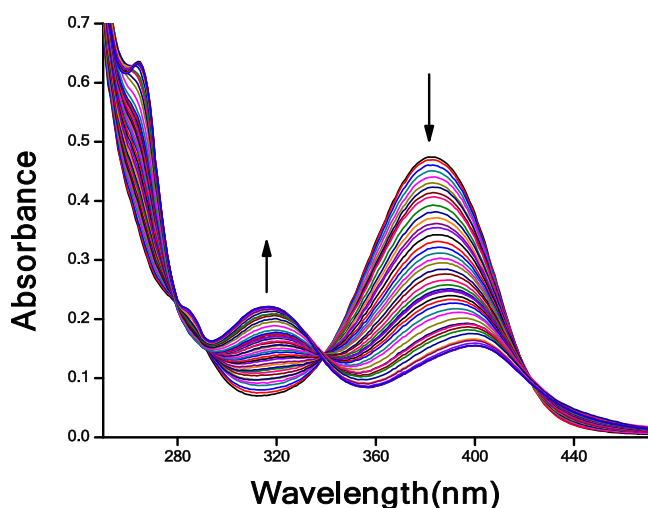

Figure 5. Analysis of the UV−visible spectrum of the complex (c = 1.0 × 10^{-5} M) with cyanide (c = 1.0 × 10^{-4} M) in a tris buffer solution (pH 7.4).

and the emission intensities of EB−DNA in the presence and absence of the quencher, respectively.[49] The slope of the linear fit plot of I^0/I versus [complex] was used to calculate the K_{sv} value. For the complex, the K_{sv} value was calculated to be 2.33 × 10^5 M^{-1} (R^2 = 0.99). Based on the equation $K_{EB}[EB]$ = K_{app}[complex] (where [EB] was taken as 5.0 × 10^{-6} M^{-1}, K_{EB} was taken as 1.0 × 10^7 M^{-1}, and a 50% reduction in the fluorescence intensity of EB was taken as the complex concentration),[50] the apparent binding constant (K_{app}) was evaluated to be 1.33 × 10^7 M^{-1} for the complex ([Ni^{II}(L)(N$_3$)]· 3H$_2$O). The high K_{app} value indicates a strong interaction between the Ni(II) complex and DNA, probably by the intercalation mechanism.

3.6. Cyanide Sensing.

3.6.1. Spectrophotometric Titration of [Ni^{II}(L)(N$_3$)]·3H$_2$O with CN$^-$. The UV−vis spectrophotometric titration was performed in an aqueous tris buffer for our complex [Ni^{II}(L)(N$_3$)]·3H$_2$O with CN$^-$. From the spectroscopic data, it is clearly seen (Figure 5) that with the gradual addition of cyanide ions (0.1 mM) into the complex solution (0.01 mM) in the aqueous buffer, at around 316 nm, a new peak emerges together with the disappearance of an old peak at

around 384 nm, yielding two isosbestic points at 339 and 280 nm. We interpret this as the displacement of ligands by cyanide ions upon the successive addition of CN$^-$ to the complex [Ni^{II}(L)(N$_3$)]·3H$_2$O.

3.6.2. Analysis of CN$^-$ Binding by Fluorescence. The fluorescence intensity of [Ni^{II}(L)(N$_3$)]·3H$_2$O with several anions was measured considering the high tendency of anions to bind to metal ions. For fluorescence titrations, we used a range of anions, e.g., CN$^-$, OAc$^-$, I$^-$, F$^-$, Br$^-$, Cl$^-$, S^{2-}, NO$_3^-$, PO$_4^{3-}$, SO$_4^{2-}$, and H$_2$PO$_4^-$, as their tetrabutyl ammonium salts along with the sodium salt of CO$_3^{2-}$, and the titrations were performed in tris buffer solution (pH 7.4). A noteworthy development of fluorescence intensity at 445 nm (Figure 6a) was detected only in the case of CN$^-$ addition. A change in color from brown to light blue was also seen by the "naked eye". The Job's plot (Figure S6) indicates a 1:2 host/guest interaction between the Ni(II) complex (host) and CN$^-$ (guest). Based on the following equation, the binding constant (K) of the complex with CN$^-$ was determined, and it was found to be 2.046 ×10^{14} M^{-2} (Figure 7a).

$$\frac{1}{F - F_0} = \frac{1}{K[CN^-]^2[F_{max} - F]} + \frac{1}{[F_{max} - F]}$$

where F, F_{max}, and F_0 are the fluorescence responses of the complex in the presence of intermediate, infinite, and zero concentrations of CN$^-$ ions, respectively. The fact that [Ni^{II}(L)(N$_3$)]·3H$_2$O displayed a relatively high selectivity for CN$^-$ compared with other anions suggests that it might make a good selective cyanide off−on chemosensor.

The emission spectrum of the free ligand was recorded, and it was compared with the fluorescence spectra of the released ligand after the reaction of the complex with CN$^-$ (Figure 6C). The position and shape of the bands in both cases were found to be identical. The emission quantum yield of the free ligand and the complex with excess CN$^-$ were measured, considering quinine sulfate as the standard, and they were found to be 0.20 and 0.14 respectively. The lower quantum yield in the latter case may be due to the presence of paramagnetic Ni(CN)$_2$ in the solution.

The selectivity of binding of CN$^-$ by [Ni^{II}(L)(N$_3$)]·3H$_2$O was investigated by the addition of CN$^-$ to solutions containing the complex and other anions, present at 5 times the molar

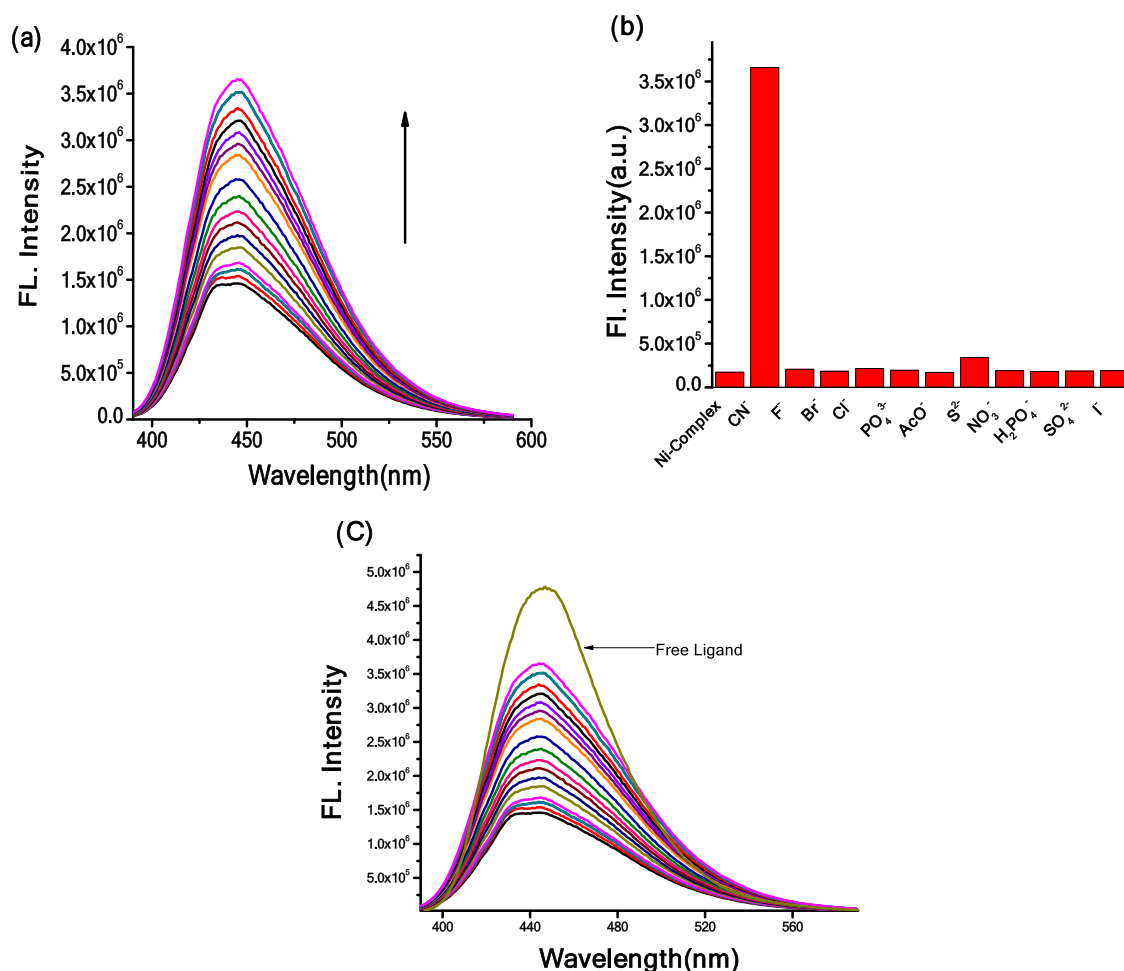**Figure 6.** (a) Fluorescence titration of $[Ni^{II}(L)(N_3)]\cdot 3H_2O$ ($c = 1.0 \times 10^{-6}$ M) with CN^- ($c = 1.0 \times 10^{-5}$ M) in tris buffer; (b) fluorescence response of the complex on adding various anions, such as CN^-, OAc^-, S^{2-}, F^-, PO_4^{3-}, Br^-, Cl^-, $H_2PO_4^-$, NO_3^-, SO_4^{2-}, and I^- in tris buffer; (c) overlay fluorescence response of the complex ($c = 1.0 \times 10^{-6}$ M) with CN^- ($c = 1.0 \times 10^{-5}$ M) and free ligand in tris buffer.

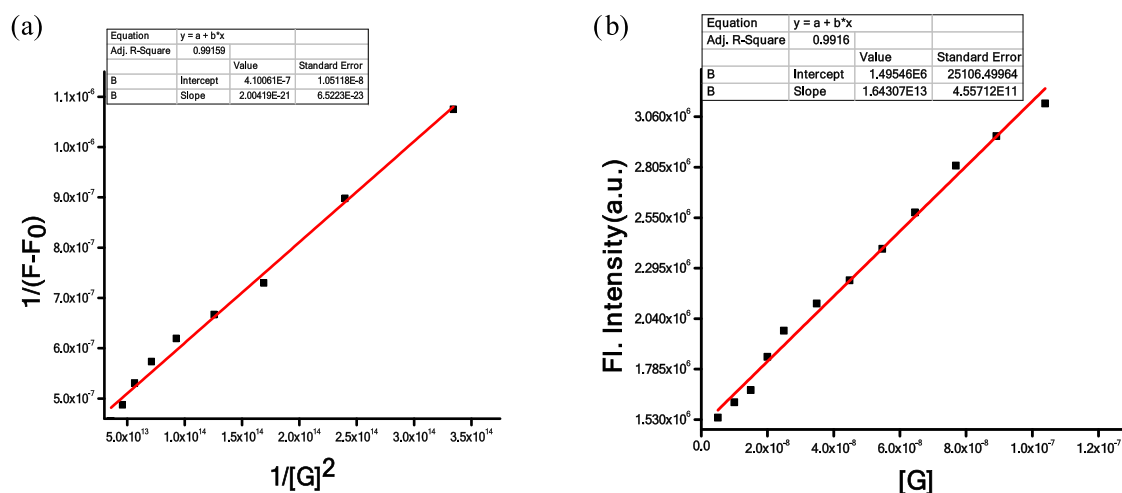**Figure 7.** (a) Determination of the binding constant of $[Ni^{II}(L)(N_3)]\cdot 3H_2O$ with cyanide; (b) determination of the detection limit of $[Ni^{II}(L)(N_3)]$ with cyanide.

equivalent of CN^-. As shown in Figure S8, although no noteworthy changes in the fluorescence response were observed in the presence of an excess of other anions, the addition of CN^- leads to significant enhancement of fluorescence under identical conditions. From the calibration curve (Figure 7b), based on K

$\times$ Sb1/S, the limit of detection for CN^- was calculated to be 9 nM with $[Ni^{II}(L)(N_3)]$ (where S is the slope, Sb1 is the standard deviation of the calibration curve, and K is a constant whose value is taken as 3 in this calculation). The limit of detection of our complex for cyanide ions was found to be significantly lower
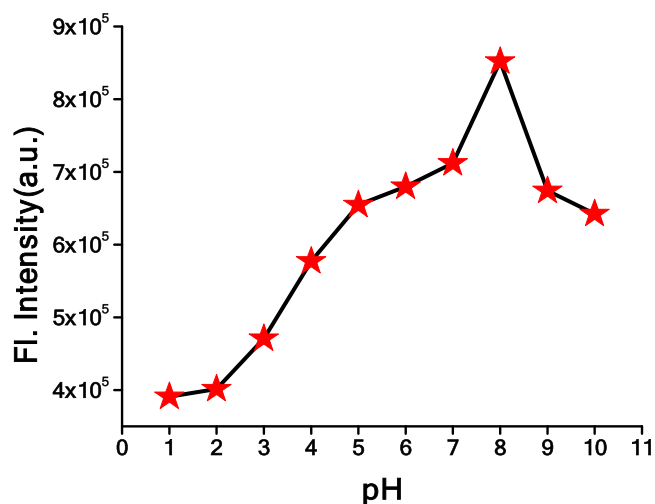
Figure 8. Maximum value of the fluorescence intensity of the complex (1×10^{-4} M^{-1}) at different pH values (λ_{em} = 445 nm).
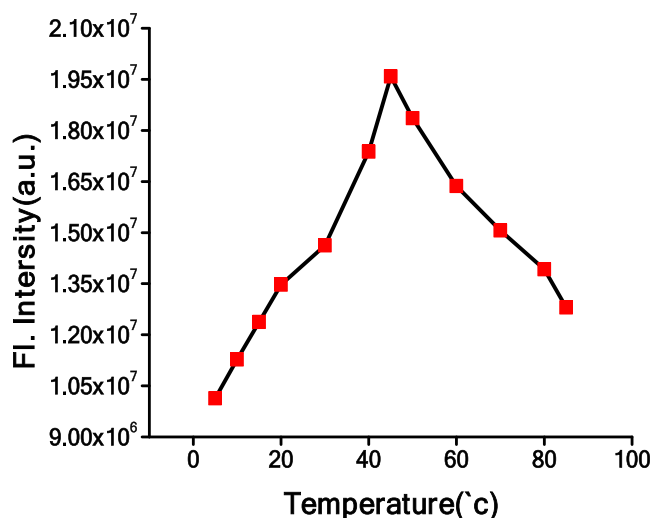

Figure 11. Maximum fluorescence intensity of the complex (0.01 μM) in the presence of 5 equiv of cyanide ions at different temperatures.
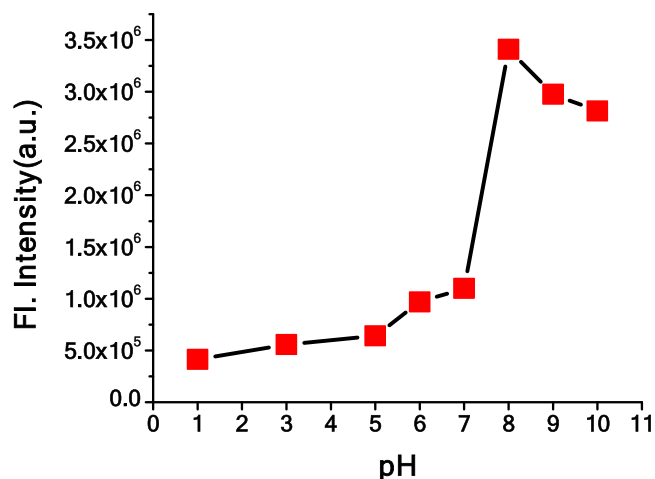

Figure 9. Maximum value of fluorescence intensity of the complex (1×10^{-4} M^{-1}) at different pH values (λ_{ex} = 384 nm) in the presence of 5 equiv of cyanide ions.

than the highest permissible value of cyanide ions (1.9 μM) recognized by WHO in drinking water.

3.6.3. Effect of pH on the Detection of CN$^-$ by the Fluorescence Method. It has been found that the fluorescence intensity of the complex and the sensing phenomena of cyanide ions are greatly influenced by the pH of the solvent. To further investigate the influence of pH on the sensing process, we prepared solutions of the complex by varying the pH over a wide range (from pH 1 to 10). At first, the fluorescence response of the Ni(II) complex in the absence of any added anion (blank) was measured, and it was plotted against pH (Figures 8 and S9). Initially, as the pH increases, the fluorescence intensity increases and reaches a peak at pH 8, but then decreases as the pH increases further.

Now, to study the pH selectivity of cyanide sensing, we performed the same experiment after adding 5 equiv of cyanide ions to each metal complex solution at different pH values and measured the fluorescence intensities (Figures 9 and S10). Here also, we plotted the fluorescence intensity against pH and, interestingly, found almost similar results, with a sharp increase
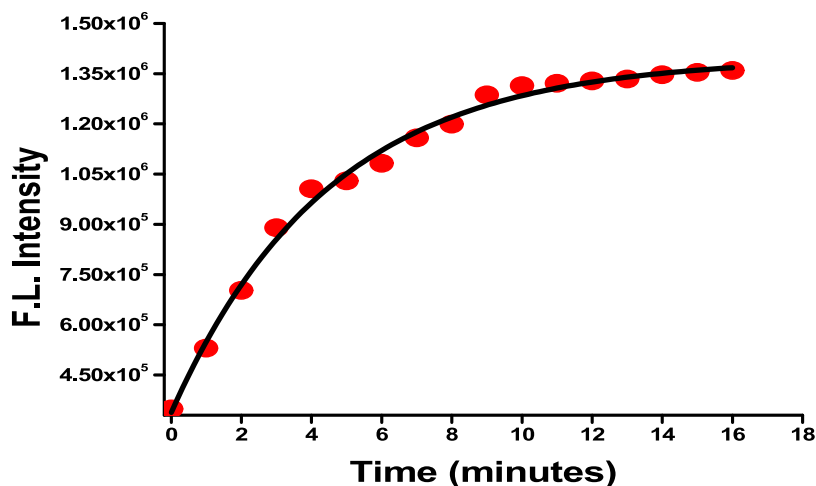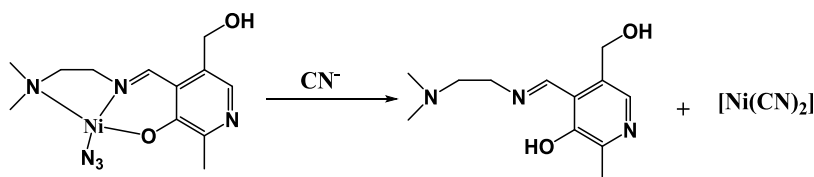

Figure 10. Fluorescence response of the complex [Ni^{II}(L)(N$_3$)]·3H$_2$O (0.1 μM) upon the addition of cyanide ions (20 equiv) as a function of time in an aqueous tris buffer solution (λ_{em} = 445 nm).

Scheme 2. Schematic Illustration of the Possible Mechanism for Detecting Cyanide

in the fluorescence intensity between pH 7 and 8, followed by a decrease.

3.6.4. Response Time of CN^- by the Fluorescence Method. To measure the response time of the Ni(II) complex toward cyanide ion binding, we took a solution of the complex (0.1 μM) in an aqueous tris buffer. Into this solution, we added 20 equiv of cyanide ion and immediately started measuring the fluorescence intensity. We measured the fluorescence response after every 1 minute and plotted the maximum fluorescence intensity against time (Figure 10). From Figure 10, it could be easily concluded that our complex started to bind with cyanide ions immediately and it took around 10 min to reach the saturation point.

3.6.5. Effect of Temperature on the Detection of CN^- by the Fluorescence Method. To investigate the effect of temperature on the sensing process, we carried out a temperature-dependent study. In this process, we added 5 equiv of cyanide ions into our Ni(II) complex solution (0.1 μM) in tris buffer (pH 7.4) (λ_{ex} = 384 nm) and measured the fluorescence intensity by changing the temperature within the range of 5−85 °C (Figure S11). Interestingly, it was found that in the initial stage, with an increase in temperature, the fluorescence response increased, reached a maximum at around 45 °C, and then decreased gradually (Figure 11). From this experiment, we can clearly conclude that our complex shows maximum affinity toward cyanide ions in the temperature range of 40−50 °C.

3.7. Possible Mode of Binding. We can anticipate that Ni^{2+} ions were captured by CN^- in tris buffer because of the high coordination ability of CN^- toward Ni^{2+}. As a result, the fluorescence of the ligand was recovered, which was earlier quenched by complexation with Ni^{2+} (Scheme 2). We verified this with an ESI−MS experiment. The ESI−MS spectrum of a reaction mixture containing the complex and CN^- shows that the predominant peak belongs to the free ligand (Figure S7), supporting our proposed mechanism.

4. CONCLUSIONS

We have reported here the synthesis of a mononuclear nickel(II) complex and its characterization, including its structure determination by X-ray crystallography. The complex can selectively detect CN^- with an l.o.d. of 9 nM. The complex also has significant binding affinity for DNA, with a K_{app} value of 1.33×10^7 M^{-1}.

■ ASSOCIATED CONTENT

ⓢ Supporting Information

The Supporting Information is available free of charge at https://pubs.acs.org/doi/10.1021/acsomega.2c04063.

Mass spectrum of the complex $[[Ni^{II}(L)(N_3)]\cdot3H_2O]$ (Figure S1); NMR spectrum of the complex $[[Ni^{II}(L)-(N_3)]\cdot3H_2O]$ (Figure S2); IR spectra of $[Ni^{II}(L)(N_3)]\cdot3H_2O$ (Figure S3); H-bonding pattern in the lattice of $[Ni^{II}(L)(N_3)]\cdot3H_2O$ (viewed along the "b" axis) (Figure S4); H-bonding pattern in the lattice of $[Ni^{II}(L)(N_3)]\cdot3H_2O$ generating plated sheets of water molecules along

the "ac" axis (viewed along the "b" axis) (Figure S5); the Job plot diagram of the complex $[[Ni^{II}(L)(N_3)]\cdot3H_2O]$ with cyanide (where X_g is the mole fraction of the guest) (Figure S6); mass spectrum of the reaction mixture of the complex $[[Ni^{II}(L)(N_3)]\cdot3H_2O]$ with excess cyanide (Figure S7); fluorescence response of $[Ni^{II}(L)(N_3)]\cdot3H_2O$ at λ_{em} = 445 nm with different anions (5 equiv, black bar) after adding CN^- (1.0 equiv, red bar) (Figure S8); fluorescence spectrum of the complex (1×10^{-4} M^{-1}) in the absence of any anion (blank) at different pH values (Figure S9); fluorescence spectrum of the complex (1×10^{-4} M^{-1}) in the presence of 5 equiv of cyanide ions at different pH values (Figure S10); fluorescence response of the complex $[Ni^{II}(L)(N_3)]\cdot3H_2O$ (0.01 μM) upon adding 5 equiv of cyanide ions at variable temperatures in tris buffer (λ_{ex} = 384 nm) (Figure S11); crystal data and refinement details of $[Ni^{II}(L)(N_3)]\cdot3H_2O$ (Table S1); some selected bond angles and bond lengths with the metal atom for the complex $[Ni^{II}(L)-(N_3)]\cdot3H_2O$ (Table S2); dimensions of hydrogen bonds (distances (Å) and angles (°)) in $[Ni^{II}(L)(N_3)]\cdot3H_2O$ (Table S3); comparison of the detection limit with previously reported methods for cyanide detection (Table S4)(PDF)

Publication of your CIF in IUCr journals; publication of your CIF in other journals (CIF)

Check CIF have been supplied for datablock(s) mbni3_0m (PDF)

■ AUTHOR INFORMATION

Corresponding Author

Shyamal Kumar Chattopadhyay − *Department of Chemistry, Indian Institute of Engineering Science and Technology, Howrah 711103, India;* ⓞ orcid.org/0000-0002-9726-922X; Email: shc20@hotmail.com, shyamal@chem.iiests.ac.in

Author

Antu Mondal − *Department of Chemistry, Indian Institute of Engineering Science and Technology, Howrah 711103, India*

Complete contact information is available at:
https://pubs.acs.org/10.1021/acsomega.2c04063

Notes

The authors declare no competing financial interest.

■ REFERENCES

(1) Douglas, C. D.; Ngu, T. T.; Kaluarachchi, H.; Zamble, D. B. Metal Transfer within the *E. Coli* HypB-HypA Complex of Hydrogenase Accessory Proteins. *Biochemistry* **2013**, *52*, 6030−6039.

(2) Ragsdale, S. W. Nickel-Based Enzyme Systems. *J. Biol. Chem.* **2009**, *284*, 18571−18575.

(3) Sigel, A.; Sigel, H.; Sigel, R. K. O.*Nickel and Its Surprising Impact in Nature*; John Wiley & Sons, Ltd.: Chichester, U. K., 2007.

(4) Calabrese, E. J.; Canada, A. T.; Sacco, C. Trace Elements and Public Health. *Annu. Rev. Public Health* **1985**, *6*, 131−146.

(5) Sharma, A. D. Relationship between Nickel Allergy and Diet. *Indian J. Dermatol. Venereol. Leprol.* **2007**, *73*, 307−312.

(6) Phipps, T.; Tank, S. L.; Wirtz, J.; Brewer, L.; Coyner, A.; Ortego, L. S.; Fairbrother, A. Essentiality of Nickel and Homeostatic Mechanisms for Its Regulation in Terrestrial Organisms. *Environ. Rev.* **2002**, *10*, 209−261.

(7) Chevin, J. C.; Maincent, P.; Mougeolle, J. M.; Jacque, M.; Martin, J. A. Nickel(II) Elimination and Autoradiographic Distribution in Normal and Nickel-Sensitized Guinea Pigs. *Int. J. Pharm.* **1988**, *45*, 101−110.

(8) Jeong, A. R.; Shin, J. W.; Jeong, J. H.; Bok, K. H.; Kim, C.; Jeong, D.; Cho, J.; Hayami, S.; Min, K. S. Dinuclear Iron (III) and Nickel(II) Complexes Containing N-(2-Pyridylmethyl)-N′-(2-Hydroxyethyl)-Ethylenediamine: Catalytic Oxidation and Magnetic Properties. *Chem. - Eur. J.* **2017**, *23*, 3023−3033.

(9) Ahn, H. M.; Bae, J. M.; Kim, M. J.; Bok, K. H.; Jeong, H. Y.; Lee, S. J.; Kim, C. Synthesis, Characterization, and Efficient Catalytic Activities of a Nickel (II) Porphyrin: Remarkable Solvent and Substrate Effects on Participation of Multiple Active Oxidants. *Chem. - Eur. J.* **2017**, *23*, 11969−11976.

(10) Barman, S. K.; Lloret, F.; Mukherjee, R. A Bioinspired Dinickel (II) Hydrolase: Solvent Vapor-Induced Hydrolysis of Carboxyesters under Ambient Conditions. *Inorg. Chem.* **2016**, *55*, 12696−12706.

(11) Kermagoret, A.; Braunstein, P. Mono- and Dinuclear Nickel Complexes with Phosphino-, Phosphinito-, and Phosphonitopyridine Ligands: Synthesis, Structures, and Catalytic Oligomerization of Ethylene. *Organometallics* **2008**, *27*, 88−99.

(12) Speiser, F.; Braunstein, P.; Saussine, L. Dinuclear Nickel Complexes with Bidentate N, O Ligands: Synthesis, Structure, and Catalytic Oligomerization of Ethylene. *Inorg. Chem.* **2004**, *43*, 4234−4240.

(13) Zhàng, D.; Jin, G. X. Novel, Highly Active Binuclear 2,5-Disubstituted Amino-p-Benzoquinone- Nickel (II) Ethylene Polymerization Catalysts. *Organometallics* **2003**, *22*, 2851−2854.

(14) Thompson, J. P.; Marrs, T. C. Hydroxocobalamin in Cyanide Poisoning. *Clin. Toxicol.* **2012**, *50*, 875−885.

(15) Vogel, S. N.; Sultan, T. R.; ten Eyck, R. P. Cyanide Poisoning. *Clin. Toxicol.* **1981**, *18*, 367−383.

(16) Parker-Cote, J. L.; Rizer, J.; Vakkalanka, J. P.; Rege, S.; Holstege, C. P. Challenges in the Diagnosis of Acute Cyanide Poisoning. *Clin. Toxicol.* **2018**, *56*, 609−617.

(17) Wilson, J. Cyanide in Human Disease: A Review of Clinical and Laboratory Evidence. *Toxicol. Sci.* **1983**, *3*, 397−399.

(18) Yang, Y. K.; Tae, J. Acridinium Salt Based Fluorescent and Colorimetric Chemosensor for the Detection of Cyanide in Water. *Org. Lett.* **2006**, *8*, 5721−5723.

(19) Li, J.; Qi, X.; Wei, W.; Liu, Y.; Xu, X.; Lin, Q.; Dong, W. A "Donor-Two-Acceptor" Sensor for Cyanide Detection in Aqueous Solution. *Sens. Actuators, B* **2015**, *220*, 986−991.

(20) Huang, X.; Gu, X.; Zhang, G.; Zhang, D. A Highly Selective Fluorescence Turn-on Detection of Cyanide Based on the Aggregation of Tetraphenylethylene Molecules Induced by Chemical Reaction. *Chem. Commun.* **2012**, *48*, 12195−12197.

(21) Lv, X.; Liu, J.; Liu, Y.; Zhao, Y.; Sun, Y. Q.; Wang, P.; Guo, W. Ratiometric Fluorescence Detection of Cyanide Based on a Hybrid Coumarin-Hemicyanine Dye: The Large Emission Shift and the High Selectivity. *Chem. Commun.* **2011**, *47*, 12843−12845.

(22) Guliyev, R.; Buyukcakir, O.; Sozmen, F.; Bozdemir, O. A. Cyanide Sensing via Metal Ion Removal from a Fluorogenic BODIPY Complex. *Tetrahedron Lett.* **2009**, *50*, 5139−5141.

(23) Mondal, A.; Das, C.; Corbella, M.; Bauzá, A.; Frontera, A.; Saha, M.; Mondal, S.; Das Saha, K.; Chattopadhyay, S. K. Biological Promiscuity of a Binuclear Cu (II) Complex of Aminoguanidine Schiff Base: DNA Binding, Anticancer Activity and Histidine Sensing Ability of the Complex. *New J. Chem.* **2020**, *44*, 7319.

(24) Kang, J. H.; Lee, S. Y.; Ahn, H. M.; Kim, C. A Novel Colorimetric Chemosensor for the Sequential Detection of Ni^{2+} and CN^- in Aqueous Solution. *Sens. Actuators, B* **2017**, *242*, 25−34.

(25) Sarre, S.; van Belle, K.; Smolders, I.; Krieken, G.; Michotte, Y. The Use of Microdialysis for the Determination of Plasma Protein Binding of Drugs. *J. Pharm. Biomed. Anal.* **1992**, *10*, 735−739.

(26) Mazloum, M.; Niassary, M. S.; Amini, M. K. Pentacyclooctaaza as a Neutral Carrier in Coated-Wire Ion-Selective Electrode for Nickel (II). *Sens. Actuators, B* **2002**, *82*, 259−264.

(27) Jankowski, K.; Yao, J.; Kasiura, K.; Jackowska, A.; Sieradzka, A. Multielement Determination of Heavy Metals in Water Samples by Continuous Powder Introduction Microwave-Induced Plasma Atomic Emission Spectrometry after Preconcentration on Activated Carbon. *Spectrochim. Acta, Part B* **2005**, *60*, 369−375.

(28) Zendelovska, D.; Pavlovska, G.; Cundeva, K.; Stafilov, T. Electrothermal Atomic Absorption Spectrometric Determination of Cobalt, Copper, Lead and Nickel Traces in Aragonite Following Flotation and Extraction separation. *Talanta* **2001**, *54*, 139−146.

(29) Sunil, A.; Rao, S. J. First Derivative Spectrophotometric Determination of Copper (II) and Nickel (II) Simultaneously Using 1-(2-Hydroxyphenyl)Thiourea. *J. Anal. Chem.* **2015**, *70*, 154−158.

(30) Anzenbacher, P.; Try, A. C.; Miyaji, H.; Jursikova, K.; Lynch, V. M.; Marquez, M.; Sessler, J. L. Fluorinated Calix [4] Pyrrole and Dipyrrolylquinoxaline: Neutral Anion Receptors with Augmented Affinities and Enhanced Selectivities. *J. Am. Chem. Soc.* **2000**, *122*, 10268−10272.

(31) Miyaji, H.; Sato, W.; Sessler, J. L. Naked-Eye Detection of Anions in Dichloromethane: Colorimetric Anion Sensors Based on Calix [4] pyrrole. *Angew. Chem., Int. Ed.* **2000**, *39*, 1777−1780.

(32) Zhou, L. L.; Sun, H.; Li, H. P.; Wang, H.; Zhang, X. H.; Wu, S. K.; Lee, S. T. A Novel Colorimetric and Fluorescent Anion Chemosensor Based on the Flavone Quasi-Crown Ether-Metal Complex. *Org. Lett.* **2004**, *6*, 1071−1074.

(33) Fabbrizzi, L.; Licchelli, M.; Rabaioli, G.; Taglietti, A. The Design of Luminescent Sensors for Anions and Ionisable Analytes. *Coord. Chem. Rev.* **2000**, *205*, 85−108.

(34) Tomasulo, M.; Sortino, S.; White, A. J. P.; Raymo, F. M. Chromogenic Oxazines for Cyanide Detection. *J. Org. Chem.* **2006**, *71*, 744−753.

(35) Singh, A.; Yao, Q.; Tong, L.; Clark Still, W.; Sames, D. Combinatorial Approach to the Development of Fluorescent Sensors for Nanomolar Aqueous Copper. *Tetrahedron Lett.* **2000**, *41*, 9601−9605.

(36) Rico, A. J.; Crooks, R. M.; Janata, J. Chemical Sensors: A Perspective of the Present and Future. *Electrochem. Soc. Interface* **1998**, *7*, 18.

(37) Park, G. J.; You, G. R.; Choi, Y. W.; Kim, C. A naked-eye chemosensor for simultaneous detection of iron and copper ions and its copper complex for colorimetric/fluorescent sensing of cyanide. *Sens. Actuators, B* **2016**, *229*, 257−271.

(38) Wang, D.; Zheng, J. Q.; Yan, X.; Zheng, X. J.; Jin, L. P. Cu (II) Complex-Based Fluorescence Chemosensor for Cyanide in Aqueous Media. *RSC Adv.* **2015**, *5*, 64756−64762.

(39) Rhaman, M. M.; Hasan, M. H.; Ali, Z. A.; Powell, D. R.; Tandon, R.; Wong, B. M.; Hossain, M. A. Charge-Density Induced Discrimination of Halides with a Rigid Dinuclear Copper(II) Complex. *Mol. Syst. Des. Eng.* **2020**, *5*, 996−1002.

(40) Rhaman, M. M.; Alamgir, A.; Wong, B. M.; Powell, D. R.; Hossain, M. A. A Highly Efficient Dinuclear Cu (II) Chemosensor for Colorimetric and Fluorescent Detection of Cyanide in Water. *RSC Adv.* **2014**, *4*, 54263−54267.

(41) Das, C.; Mondal, A.; Sengupta, S.; Cardin, C.; Chattopadhyay, S. K. Selective Cyanide Sensing Using a Fe (III) Complex of Pyridoxal-Beta Alanine Schiff Base. *Spectrochim. Acta, Part A* **2022**, *273*, No. 120943.

(42) Mondal, S.; Chakraborty, M.; Mondal, A.; Pakhira, B.; Blake, A. J.; Sinn, E.; Chattopadhyay, S. K. Cu (II) Complexes of a Tridentate N,N,O-Donor Schiff Base of Pyridoxal: Synthesis, X-Ray Structures, DNA-Binding Properties and Catecholase Activity. *New J. Chem.* **2018**, *42*, 9588−9597.

(43) Sheldrick, G. M. A short history of SHELX. *Acta Crystallogr., Sect. A: Found. Crystallogr.* **2008**, *64*, 112−122.

(44) Sheldrick, G. M. Crystal structure refinement with SHELXL. *Acta Crystallogr., Sect. C: Struct. Chem.* **2015**, *71*, 3−8.

(45) Howe-Grant, M.; Lippard, S. J.; Wu, K. C.; Bauer, W. R. Binding of Platinum and Palladium Metallointercalation Reagents and Antitumor Drugs to Closed and Open DNAs. *Biochemistry* **1976**, *15*, 4339−4346.

(46) Meyer-Almes, F. J.; Porschke, D. Mechanism of Intercalation into the DNA Double Helix by Ethidium. *Biochemistry* **1993**, *32*, 4246−4253.

(47) Indumathy, R.; Radhika, S.; Kanthimathi, M.; Weyhermuller, T.; Nair, B. U. Cobalt Complexes of Terpyridine Ligand: Crystal Structure and Photocleavage of DNA. *J. Inorg. Biochem.* **2007**, *101*, 434−443.

(48) Kumar, R. S.; Arunachalam, S.; Periasamy, V. S.; Preethy, C. P.; Riyasdeen, A.; Akbarsha, M. A. Surfactant−Cobalt (III) Complexes: Synthesis, Critical Micelle Concentration (CMC) Determination, DNA Binding, Antimicrobial and Cytotoxicity Studies. *J. Inorg. Biochem.* **2009**, *103*, 117−127.

(49) Tabassum, S.; Parveen, S.; Arjmand, F. New Modulated Metallic Macrocycles: Electrochemistry and Their Interaction with Calf Thymus DNA. *Acta Biomater.* **2005**, *1*, 677−689.

(50) Lee, M.; Rhodes, A. L.; Wyatt, M. D.; Forrow, S.; Hartley, J. A. GC Base Sequence Recognition by Oligo (Imidazolecarboxamide) and C-Terminus-Modified Analogues of Distamycin Deduced from Circular Dichroism, Proton Nuclear Magnetic Resonance, and Methidiumpropylethylenediaminetetraacetate-Iron (II) Footprinting Studies. *Biochemistry* **1993**, *32*, 4237−4245.